COMMUNICATION

Enhanced UV-light stability of planar heterojunction perovskite solar cells with caesium bromide interface modification†

Wenzhe Li,‡[ab] Wei Zhang,‡[a] Stephan Van Reenen,[a] Rebecca J. Sutton,[a] Jiandong Fan,[a] Amir A. Haghighirad,[a] Michael B. Johnston,[a] Liduo Wang*[b] and Henry J. Snaith*[a]

Interfacial engineering has been shown to play a vital role in boosting the performance of perovskite solar cells in the past few years. Here we demonstrate that caesium bromide (CsBr), as an interfacial modifier between the electron collection layer and the $CH_3NH_3PbI_{3-x}Cl_x$ absorber layer, can effectively enhance the stability of planar heterojunction devices under ultra violet (UV) light soaking. Additionally, the device performance is improved due to the alleviated defects at the perovskite-titania heterojunction and enhanced electron extraction.

The global energy demand has grown significantly over the last decades and the conversion of solar energy into electricity represents one of the most promising routes to meet this demand.[1,2] Organic–inorganic lead halide perovskite materials, such as $CH_3NH_3PbI_3$, have been used in solar cells because of their multiple capabilities of light absorption, charge separation, and long range transport of both holes and electrons.[3–10] In 2012, the stability of perovskite solar cells (PSCs) was improved significantly by replacing the liquid electrolyte used in the first embodiments with the organic hole-transport material (HTM) 2,2′,7,7′-tetrakis(*N*,*N*-di-*p*-methoxyphenyl-amine)-9,9′-spirobifluorene (spiro-OMeTAD). This also resulted in an unexpected power conversion efficiency (PCE) of up to 9.7% and 10.7% based on mesoporous TiO_2 and Al_2O_3 structures, respectively.[4,11] In parallel to the mesoporous architecture, planar heterojunction solar cell structures have also been developed where a solid film of the perovskite material is sandwiched between the electron and hole collection layers, fabricated *via* either solution processing or vapour deposition techniques, showing respectable PCEs of above 19%.[6,9,12,13] This kind of solar cell architecture has several advantages as compared to the mesoscopic structure,

Broader context

Organic–inorganic lead halide perovskite solar cells are fast becoming high-performance low-cost competitors to the dominant silicon solar cells, but they still face some challenges for commercialisation. Despite rapid improvement in the device performance of perovskite solar cells over the past few years, there remains an intrinsic instability of the perovskite materials when in contact with non-benign material interfaces and this poses a key issue for the long term stability of devices. Here we demonstrate CsBr as an interfacial modifier between the electron collection layer and the $CH_3NH_3PbI_{3-x}Cl_x$ perovskite absorber layer. By this modification we achieve enhancement of the device performance as well as stability under ultra violet (UV) light soaking. Our results highlight the potential of interfacial modification in achieving long term stability of perovskite solar cells incorporating n-type TiO_2 or other metal oxides.

such as a simpler structure, versatile fabrication routes, and tuneable crystal grain size.[12,14,15] The current highest certified PCE of 20.1% for PSCs was achieved through the material composition engineering technique and the marriage of mesoporous and planar heterojunction solar cell architecture, where a very thin (150 nm) mesoporous TiO_2 film is infiltrated and coated with around a 500 nm thick solid perovskite film.[16] The fast PCE growth of PSCs indicates their great potential to become competitive to traditional silicon solar cells and other thin-film solar cells in the next few years.[17–21]

In the planar heterojunction structure, typically a thin TiO_2 compact layer (c-TiO_2), perovskite layer and spiro-OMeTAD form an n–i–p heterojunction.[6] However, despite the relatively low surface area of contact between the perovskite and the p and n-type collection layers, these planar cells remain very sensitive to the interfaces, in particular, between c-TiO_2 and $CH_3NH_3PbI_3$. As previously illustrated, the present research on PSCs mainly focuses on high performance *via* different device structures, materials and fabrication methods.[22] However, a key issue for the deployment of PSCs in industry is not just to enhance the PCE, but also to increase the photovoltaic stability and understand the underlying mechanism that could lead to instability. In previous works, the perovskite film instability in moisture and

490 | *Energy Environ. Sci.*, 2016, **9**, 490–498

This journal is © The Royal Society of Chemistry 2016

the corresponding degradation mechanism has been assessed.[23] For instance, the addition of an Al_2O_3 layer on top of the perovskite capping layer has been found to enhance the perovskite stability in moisture.[24,25] In the perspective of development of perovskite material, partially substituting some of the iodide in perovskite with bromide could improve both efficiency and humidity stability.[26] Smith *et al.* used $(PEA)_2(MA)_2[Pb_3I_{10}]$ (PEA: $C_6H_5(CH_2)_2NH_3^+$, MA: $CH_3NH_3^+$) as the absorber and fabricated hybrid perovskite solar cells with enhanced moisture stability.[27] In addition, as for the HTM, the most frequently used material spiro-OMeTAD, doped with Li-TFSI and tBP,[4,6] is moisture sensitive and will compromise the device stability. In this context, Habisreutinger *et al.* showed that by using carbon nanotubes and PMMA as the HTL, the water and thermal stability of the PSCs could be improved.[28] In addition, hole-conductor-free devices using carbon electrode showed stable device performance over 1000 hours in ambient air under full sunlight.[29]

To date, most stability studies focused on the effect of moisture and to a certain extent heat, and the effect of UV light is less investigated. A reduced stability under UV light has been observed and attributed to changes occurring in the c-TiO_2 and/or mesoporous TiO_2 layers, which are widely used in high performance perovskite solar cells.[30] This is especially prevalent when the cells are encapsulated from atmospheric oxygen. Upon UV light exposure, photo generated holes in the mesoporous TiO_2 react with oxygen absorbed at surface oxygen vacancies, which then become deep traps leading to charge recombination.[31] We have demonstrated that by replacing mesoporous TiO_2 with mesoporous Al_2O_3 a significant improvement of the UV stability in the solar cell is achieved.[31] Ito and co-workers introduced a blocking layer of Sb_2S_3 between mesoporous TiO_2 and perovskite layers, which improved light stability of devices.[30] However, Sb_2S_3 is relatively toxic and unstable in the environment with oxygen and moisture, and in addition requires curing at 300 °C. More recently we have shown that in the planar heterojunction solar cells, the c-TiO_2 collection layers still persist to induce photocurrent degradation when encapsulated and stressed under load under full spectrum sunlight.[32,33] There is hence a requirement to improve the stability of c-TiO_2 if it is to be useful for the long term operation of perovskite solar cells.

Herein, we demonstrate that CsBr can be employed as an interface modifier for the c-TiO_2. The CsBr modification (coating) reduces the areal density of pin-holes through to the FTO and results in a negative shift in the work of function of c-TiO_2 from 4.07 to 3.90 eV. Most significantly, the CsBr modification dramatically inhibits UV induced degradation of the perovskite films and devices, which we do observe to occur with the unmodified c-TiO_2. Our study indicates that the improved UV stability arises from reduced photocatalytic properties of the TiO_2 and reduced electronic defect density at the c-TiO_2/perovskite heterojunction. In addition, despite the apparent unfavourable direction of the shift in surface potential, the CsBr interface modification increases the electron transfer rate from the perovskite to the c-TiO_2, leading to a measureable improvement of the PCE.

We start from studying the morphology of CsBr on c-TiO_2 layer based on a coloration method using $AgNO_3$ as the indicator.
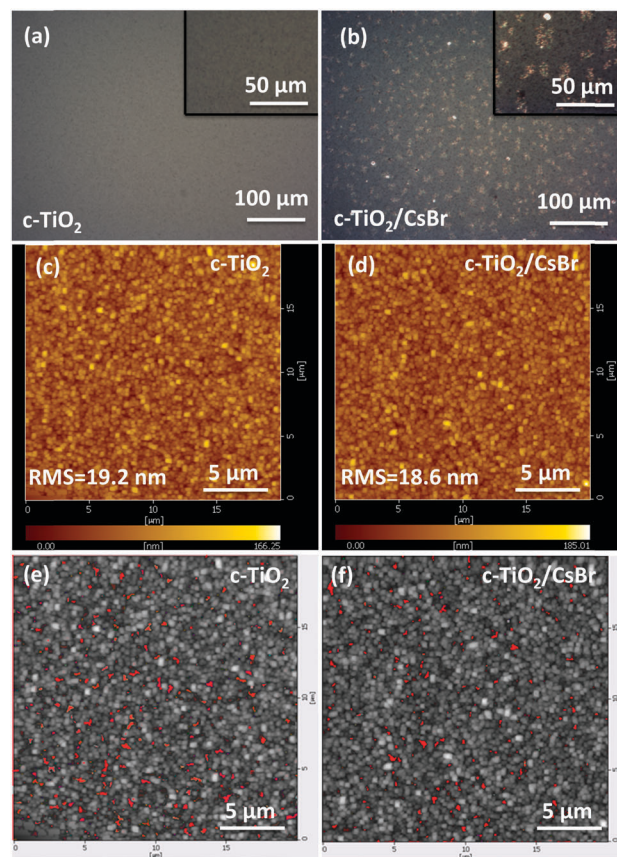

Fig. 1 Microphotographs of (a) TiO_2 compact layer (c-TiO_2) and (b) c-TiO_2/CsBr substrates after coloration. AFM topography of a c-TiO_2 on FTO glass without (c) and with (d) CsBr modification; (e) and (f) show the corresponding height mapping.

In brief, CsBr will react with $AgNO_3$ to form AgBr, which further degrades into Ag under UV light irradiation (see experimental section for more details). In Fig. 1 we show microphotographs of c-TiO_2 substrates without (Fig. 1a) and with (Fig. 1b) CsBr modification after coloration. The presence of bright clusters in Fig. 1b indicates that CsBr forms clusters on the surface of c-TiO_2, similar to Cs_2CO_3,[34] rather than a continuous film on the c-TiO_2 surface. We further investigated the morphology of the c-TiO_2 on FTO glass without and with CsBr modification *via* atomic force microscopy (AFM), which we show in Fig. 1c and d. The bare c-TiO_2 on FTO glass is relatively smooth with homogenous aggregation of TiO_2 nanocrystals (Fig. 1c), showing a root mean square (RMS) roughness of 19.2 ± 0.5 nm over an area of 400 μm^2. We note that in previous work we have estimated the "porosity" of the c-TiO_2 layers fabricated *via* this route to be approximately 4%,[35] so they are not entirely continuous. After CsBr modification (Fig. 1d), we observe that the RMS value decreases marginally to 18.6 ± 0.6 nm. In Fig. 1e and f we show the corresponding height mapping extracted using image software. After CsBr modification, the ratio of uncovered FTO area to the whole substrate decreases from 3.1% to 1.1%. These results demonstrate that CsBr modification improves the film smoothness and at the same time partially blocks the pinholes in the c-TiO_2.

This journal is © The Royal Society of Chemistry 2016

Energy Environ. Sci., 2016, **9**, 490–498 | 491

We further interrogated the c-TiO$_2$ layers *via* ultraviolet photoelectron spectroscopy (UPS) which we show in Fig. 2a, in order to ascertain if there is any change of the energy levels of the c-TiO$_2$ before and after CsBr modification. We observe that the work function of the TiO$_2$ drops from 4.07 to 3.90 eV after CsBr modification. Coating a metal oxide with a thin layer of another material can often induce a shift in the energy levels due to modification to the surface states on the oxide, or charge transfer between the modifier and the metal oxide.[36,37] The work function change which we observe here could be attributed to the doping of the surface of the c-TiO$_2$ with the CsBr. Similar phenomena have been extensively observed with Cs$_2$CO$_3$, having been employed as a surface modifier for c-TiO$_2$ in both organic light emitting diodes and photovoltaics.[34] The decrease of the work function of the c-TiO$_2$ could increase the built-in potential inside the devices, which could hence lead to the increased open-circuit voltage. However, we have previously observed poor

electron extraction from the perovskite absorbers into c-TiO$_2$, which we would expect to get worse with a reduction in the energy level of the conduction band edge.[38] We will return to this point later in the manuscript. In Fig. 2b we illustrate the energy level diagram of the FTO/TiO$_2$(CsBr)/perovskite interface where we highlight that the conduction band of TiO$_2$ is shifted by around 0.2 eV towards the vacuum level after CsBr modification. For completeness we also show the energy levels of the spiro-OMeTAD hole-conductor and Au, which will be employed in the complete solar cells later on in the manuscript.

For the work here we employ our standard "mixed halide" perovskite MAPbI$_{3-x}$Cl$_x$ which is processed from methylammonium iodide (MAI) : PbCl$_2$ at a 3 : 1 molar ratio in DMF. We process the CsBr from a mixed solvent of isopropanol and water, and we note that it is not soluble in DMF. In Fig. S1 (ESI†) we show the light absorption spectra of MAPbI$_{3-x}$Cl$_x$ perovskite films coated upon FTO/c-TiO$_2$ substrates modified with CsBr cast from solutions of different concentrations. The absorption is slightly enhanced at short wavelengths and near the band edge when increasing the concentration of the CsBr solution from 0.1 to 10 mg mL^{-1}.

The enhanced absorbance is unlikely to be due to a change in the overall thickness of the films since it is not panchromatic and we estimate a thickness increase of only 423 *versus* 412 nm *via* measuring 50 positions in the cross-section images, as shown in Fig. S4a and S4b (ESI†).[39] The absorbance in the region where the perovskite absorbs very strongly, at the range of 350–600 nm, is directly influenced by the density of pinholes larger than the wavelength of light. For example if there was a 1% density of large pinholes, we would expect a maximum optical density (OD) in a thick film to be 2.[40] Hence, small changes to the surface coverage could result in changes to the optical density in this region. For all the films processed here the surface coverage is very high (OD > 2.5), but we do observe some pinholes in the films processed on unmodified TiO$_2$, which are not present in the films processed on the CsBr modified c-TiO$_2$. With the increase of CsBr concentration, the absorbance in the excitonic peak near the band edge is significantly enhanced. This is consistent with increased average crystal domain size and/or crystallinity, which indicates fewer grain boundaries in the perovskite films and a favourable surface for more uniform crystalisation.[41]

We show the X-ray diffraction (XRD) patterns in Fig. 2c of perovskite films processed on c-TiO$_2$ modified with 2.5 mg mL^{-1} CsBr solution and control perovskite films fabricated on unmodified FTO/c-TiO$_2$ substrates. The spectra are normalized by the FTO peaks at 26.25° and 37.48°. With CsBr modification, the diffraction peaks for the MAPbI$_{3-x}$Cl$_x$ perovskite do not contain any detectable shifts or new peaks in comparison to the control films. If the caesium perovskite, CsPbBr$_{3-x}$I$_x$ was forming near the interface, we would expect to observe new diffraction peaks associated with the CsPbBr$_3$ perovskite, for which we show the simulated diffraction pattern in the top panel of Fig. 2c. In order to clarify whether the CsBr can react with the perovskite precursor solution, we deposited a nearly 200 nm thick CsBr layer on c-TiO$_2$ and subsequently coated the film with PbCl$_2$/MAI with
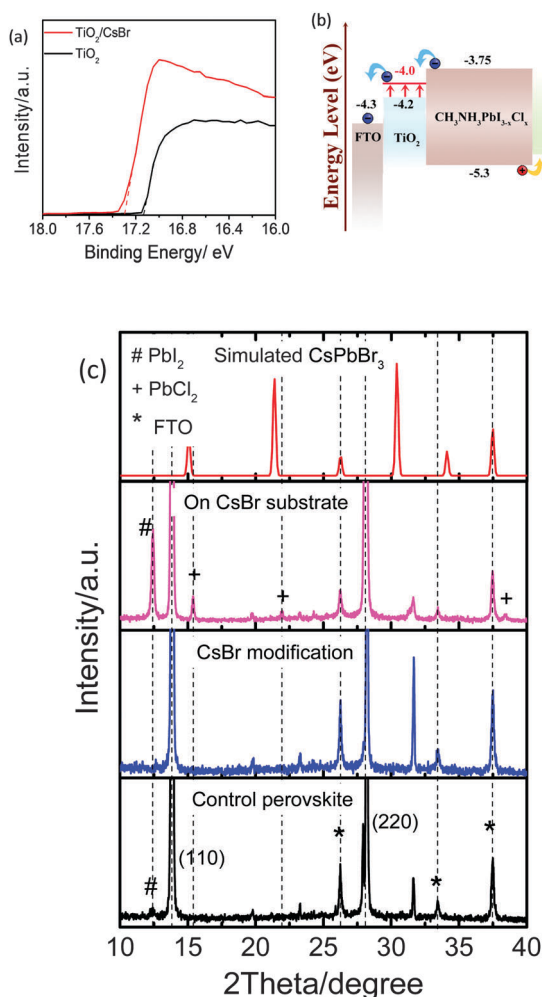

Fig. 2 (a) UPS spectra of c-TiO$_2$ with (w) and without (w/o) CsBr modification. The light source of UPS is a He1 discharge lamp (*hν* = 21.2 eV); (b) energy level diagram of the device with the structure of FTO/c-TiO$_2$(CsBr)/perovskite/spiro-OMeTAD/Au; (c) X-ray diffraction spectra of control perovskite on c-TiO$_2$ (black line), perovskite on c-TiO$_2$ with thin CsBr modification layer (blue line), perovskite on c-TiO$_2$ with thick CsBr modification layer (pink line) and simulated XRD data for bulk CsPbBr$_3$ material (red line).

492 | *Energy Environ. Sci.*, 2016, **9**, 490–498

This journal is © The Royal Society of Chemistry 2016

additional PbI_2 in the DMF solution, followed by annealing at 100 °C for 90 minutes. We show the XRD patterns of thick CsBr modified perovskite by the pink line in Fig. 2c. A series of new diffraction peaks located at 15.4, 22.1 and 38.4 degrees are visible for the CsBr modified perovskite, which we attribute to the diffraction of $PbCl_2$ and PbI_2, but not a newly formed Cs perovskite.[42,43] To further confirm this, we simulated the XRD pattern of $CsPbBr_3$, which has three main peaks at 15.1, 21.4 and 37.5 degrees. In general, if the larger ions are substituted with smaller ions, such as $MA^+ \rightarrow Cs^+$ or $I^- \rightarrow Br^-$, the main perovskite diffraction peaks should be shifted to larger angles, which we do not observe. The new peaks we observe when the hybrid perovskite solution is cast upon the thick CsBr layer, are most likely originating from PbI_2 impurities (at 12.42 degrees) and $PbCl_2$ impurities (at 15.39 degrees). For the $MAPbI_{3-x}Cl_x$ films processed on the thinner CsBr films, we do not observe any significant shift in the position of the XRD peaks. The notable difference is the lack of a measurable diffraction peak from PbI_2 impurity for perovskite films processed on the CsBr modified substrates. Thus, these results suggest that the CsBr does not become incorporated into the perovskite lattice, but remains as an interface modifier. We note that it is typically necessary to heat Cs based perovskite films to temperatures in excess of 250 °C in order to properly crystallise, whereas here our films are only heated to 100 °C, consistent with us not observing any phases of the $CsPbX_3$ perovskites.[44]

To investigate the optoelectronic impact of the CsBr modification, we investigate the photoluminescence of the films. In Fig. 3 we show the steady-state photoluminescence (PL) spectra

of the $CH_3NH_3PbI_{3-x}Cl_x$ films deposited on glass and c-TiO_2 layers with and without the CsBr modification. We observe the characteristic emission peak of $CH_3NH_3PbI_3$ at around 774 nm, showing a little Stokes shift in comparison with the absorbance spectrum which we show in Fig. S1 (ESI†).[45]

With CsBr coating of the glass substrates (no FTO or TiO_2), the PL intensity from the perovskite is improved by nearly 50%. We show the time-resolved PL decay of perovskite thin films deposited on glass with and without CsBr modification in Fig. 3b. We fitted the curves and obtained the corresponding decay life-times with a biexponential decay function.[46] The presence of CsBr dramatically retards the PL decay process with the fast decay component lifetime τ_{fast}, increasing from 5.0 to 20.8 ns and the slow component, τ_{slow}, from 118.0 to 177.6 ns. We show the fitting parameters in Table S1 (ESI†). This is consistent with there being fewer defects in the perovskite material crystallised upon the CsBr surface.[45,47] We further studied the electron injection process from perovskite to the c-TiO_2 by collecting the time-resolved PL spectra of the perovskite deposited on the c-TiO_2 with and without the CsBr modification. Surprisingly, in this study the PL quenching for the perovskite processed on c-TiO_2 is already quite strong. This is in contrast to other studies we have performed where we have observed relatively poor PL quenching for perovskite films processed on c-TiO_2.[33] We explain this in detail in the experimental section, but these perovskite films are dried and crystallised very slowly which results in extremely high surface coverage. This may also have a strong impact upon the defect or interface states generated during crystallisation. If the poor electronic contact, previously observed
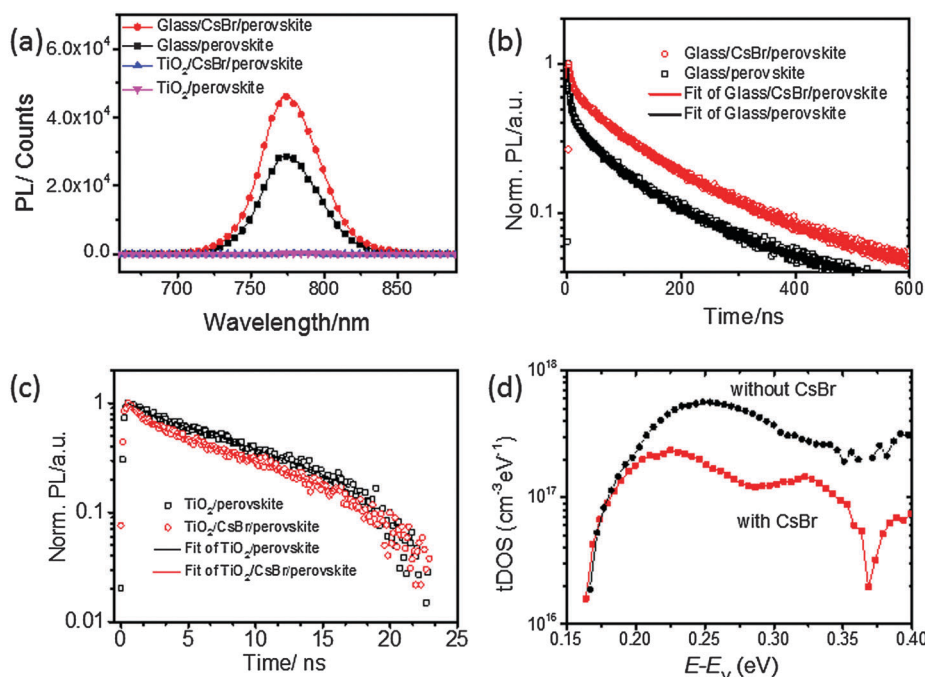

Fig. 3 (a) Steady-state photoluminescence spectra of perovskite thin films deposited on glass and c-TiO_2 layer with and without CsBr modification collected following excitation at 510 nm, (b) time-resolved photoluminescence spectra of perovskite thin films on glass collected at 400 kHz (c) and on c-TiO_2 layer collected at 30 MHz at 0.03 µJ per cm² per pulse, (d) trap density of states (tDOS) for devices without CsBr (black) and with CsBr modification (red).

between the c-TiO$_2$ and the perovskite, is predominantly resultant from a high density of defects generated within the perovskite at that interface, then improvement to the perovskite crystallisation protocol to inhibit defect formation will hence enhance the nature of the electronic contact. For the CsBr modified substrates, the PL decay is quenched even faster, with the τ_{fast} decreasing from 1.70 to 1.16 ns and τ_{slow} from 19.6 to 13.4 ns for the films processed on the CsBr modified c-TiO$_2$. We further studied the defect density at the perovskite/c-TiO$_2$ interface by performing thermal admittance spectroscopy (TAS) on complete photovoltaic devices. By interrogating the frequency dependent capacitance *via* TAS measurements we can determine the energetic profile of trap density of state (tDOS).[48,49] We show the result in Fig. 3d. We give more details on the determination of the tDOS by TAS in the ESI† Fig. S2 and S3. We found that the tDOS decreased from 5.0×10^{16} (without CsBr) to 2.0×10^{16} cm^{-3} (with CsBr), confirming that the electronic contact between perovskite and c-TiO$_2$ is enhanced through CsBr modification.

A key motivation for this work is to see if the c-TiO$_2$/perovskite interface can be modified in such a way to inhibit UV light induced degradation. For UV degradation studies, we attached perovskite films deposited on FTO/c-TiO$_2$ substrates to an optical mask with a window area of 0.79 cm^2, and exposed these masked films to UV irradiation (λ = 365 nm) with an intensity of 523 mW cm^{-2} in air. We note that there is only 4.6 mW cm^{-2} of UV light present (at wavelengths of less than 400 nm) within the AM1.5 solar spectrum at 100 mW cm^{-2} irradiance, hence our UV illumination here represents more than 100 times the solar UV irradiance. We measured the temperature of the films and devices under UV light exposure to be about 45 °C, with an IR temperature gun. We recorded the absorbance curves every 5 min after cooling down the film to room temperature. After 95 minutes of UV aging (equivalent to around 180 h of solar exposure), the normalized absorbance for the MAPbI$_{3-x}$Cl$_x$ film on glass without TiO$_2$ is still above 99% as we show in Fig. 4a. However, from 40 minutes irradiation and onwards, the absorbance of the perovskite film processed on c-TiO$_2$ falls sharply from 0.99 to 0.85. After UV aging, a peak appears at 520 nm, which we assign to PbI$_2$ absorption (bandgap of 2.6 eV). This is evident as visible degradation in the form of a yellow region in the UV exposed area which we show in Fig. 4a. The perovskite with the CsBr interface modification on c-TiO$_2$/FTO substrates performed much better than the control film. In the first 20 min, the normalized absorbance of the film shows little decay and still holds at 0.99. After 95 minutes of aging, the normalized absorption is still over 98% and the film did not present any visible sign of yellowing, as we show in Fig. 4a.

In order to study any UV light induced morphological changes in the films, we performed scanning electron microscopy (SEM). In Fig. S4a and b (ESI†), we show the cross-sectional SEM images of the planar heterojunction solar cells without and with CsBr modification layer. In Fig. S4c–f (ESI†) we show the top view images of films without and with CsBr modification and the films after 100 min UV light exposure. Before UV exposure, the control perovskite films have a rough surface with clear crystal boundary (Fig. S4c, ESI†). However, after UV aging for 100 min
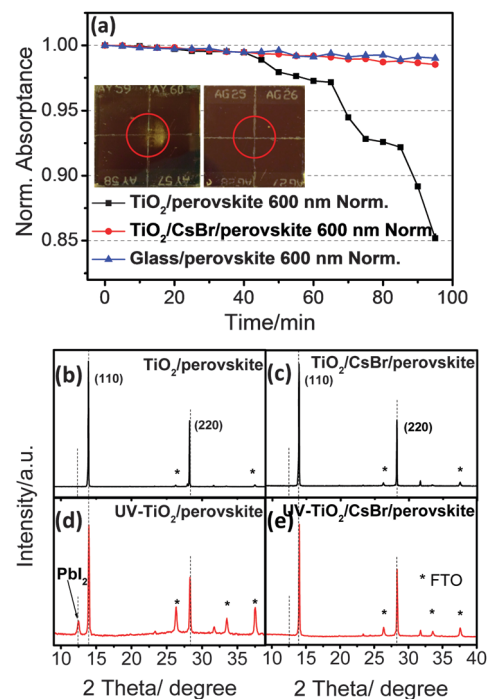

Fig. 4 (a) Normalized absorptance at 600 nm wavelength. The inset images are photographs of each film after UV aging with 523 mW cm^{-2} intensity; the red circle in the middle of film is the UV light window. XRD patterns with Cu Kα radiation (λ = 1.54056 Å) of CH$_3$NH$_3$PbI$_3$ film (b) before and (d) after UV aging for 100 min; CH$_3$NH$_3$PbI$_3$ film with CsBr layer (c) before and (e) after UV aging. * indicates the diffraction peak position of FTO reflection and # for PbI$_2$ reflections.

(Fig. S4e, ESI†), the perovskite film becomes smoother and the grain boundaries become indistinguishable. However, the morphology for the perovskite films processed upon the c-TiO$_2$/FTO substrates modified with CsBr did not change noticeably after UV aging.

We also performed XRD measurements on perovskite films with and without CsBr modification to explore the film stability and degree of degradation, as we show in Fig. 4b–e. After UV aging, we observe a new diffraction peak at 2θ = 12.49 degrees in the XRD pattern for the control perovskite, which is the (001) diffraction peak of PbI$_2$, often observed as the final degradation product from lead iodide based perovskites.[24,50] During the UV aging process, the intensity ratio of the PbI$_2$(001)/perovskite(110) diffraction peak increases from 0.001 to 0.13. For the perovskite film with CsBr modification, the relative intensity of the diffraction peak increases from 0.001 to 0.004 only. The reduced amount of by-product (PbI$_2$) demonstrates a lower degree of degradation. Thus CsBr modification effectively retards the perovskite degradation under UV light exposure.

To understand the mechanism of degradation inhibition, we further investigated the photocatalytic properties of TiO$_2$ with and without CsBr modification by tracing the absorption of methyl blue in ethanol solution under UV irradiation *versus* time according to literature report.[51] We show the result in Fig. S5 (ESI†). Please note that we employed mesoporous TiO$_2$ film herein rather than the compact TiO$_2$ since we required a

494 | *Energy Environ. Sci.*, 2016, **9**, 490–498

This journal is © The Royal Society of Chemistry 2016

large surface area of interaction between the TiO_2 and the methyl blue solution, in order to enable the measurement to be performed within a practical time. We give further details in the ESI.† We observe that methyl blue degrades much faster on pristine TiO_2 than on TiO_2 with CsBr modification, which demonstrates that CsBr effectively reduces the chemical reactivity of TiO_2 under UV light soaking. We further studied CsBr modified TiO_2 before and after the photocatalytic experiment by XPS (Fig. S6, ESI†), which indicates negligible change of the CsBr under UV light soaking. Based on these results, we infer that the mechanism for the improved UV stability is due to the dual effect of reduced chemical reactivity of TiO_2 after CsBr modification and reduced defect density at the c-TiO_2/perovskite interface, with the defect sites being the most likely sites for the onset of degradation.

Inhibiting photo-degradation is very important; however the substrate still needs to act effectively as a charge selective contact. To investigate the influence of the CsBr treatment on solar cells, we fabricated planar heterojunction solar cells and studied the effect of CsBr interface modification on device performance (we show the dependence of device performance upon CsBr concentration in Fig. S7, ESI†). As we show in Fig. 5a, we observe that the devices incorporating the CsBr modification at the optimised concentration achieved an average PCE of 15.3%, as measured *via* current voltage measurements under simulated AM1.5 sun light at 100 mW cm^{-2} irradiance, which is significantly improved as compared to the control devices with an average PCE of 11.5%.

Perovskite solar cells often exhibit hysteresis in the current voltage curves, where the derived efficiency from scanning from forward bias (FB) to short-circuit (SC) is usually higher than from scanning from SC to FB.[12,33] We have recently elucidated the precise mechanism of hysteresis through theoretical modelling, and it occurs due to a combination of the presence of mobile ions and electronic traps near the charge collection layers.[52] An effective means to determine the steady-state efficiency is to hold the cell at a fixed voltage near the maximum power point on the JV curve and measure the photocurrent generated at this fixed applied bias until it stabilizes.[53] We summarize the solar cell performance parameters in Table 1. The champion FB-SC JV determined efficiency of the planar heterojunction devices here with CsBr modification is 16.3% (Fig. S8, ESI†) which we observe to exhibit a stabilized power output (SPO) of 14.7%. We also calculated the ratio between the SPO and PCE from JV scan (JV_{PCE}). The closer the ratio is to one, the less prevalent the hysteresis. The ratio here of the SPO/JV_{PCE} for the champion cell is 0.90, which is very good for planar heterojunction cells employing c-TiO_2, indicative of a relatively low electron trap density at the c-TiO_2/perovskite interface. In comparison we determined the JV_{PCE} and SPO for the champion control cell to be 13.1% and 10.9% respectively, giving an SPO/JV_{PCE} ratio of 0.83. If our model for hysteresis is correct, then this indicates that the presence of the CsBr not only improves overall power conversion efficiency, but it also reduces hysteresis effects due to having reduced the defect density at the perovskite/c-TiO_2 interface. This is in good agreement with the TAS measurement we discussed above and presented in Fig. 3d, where we determine a reduction in trap density of states for the cells with the CsBr modification.
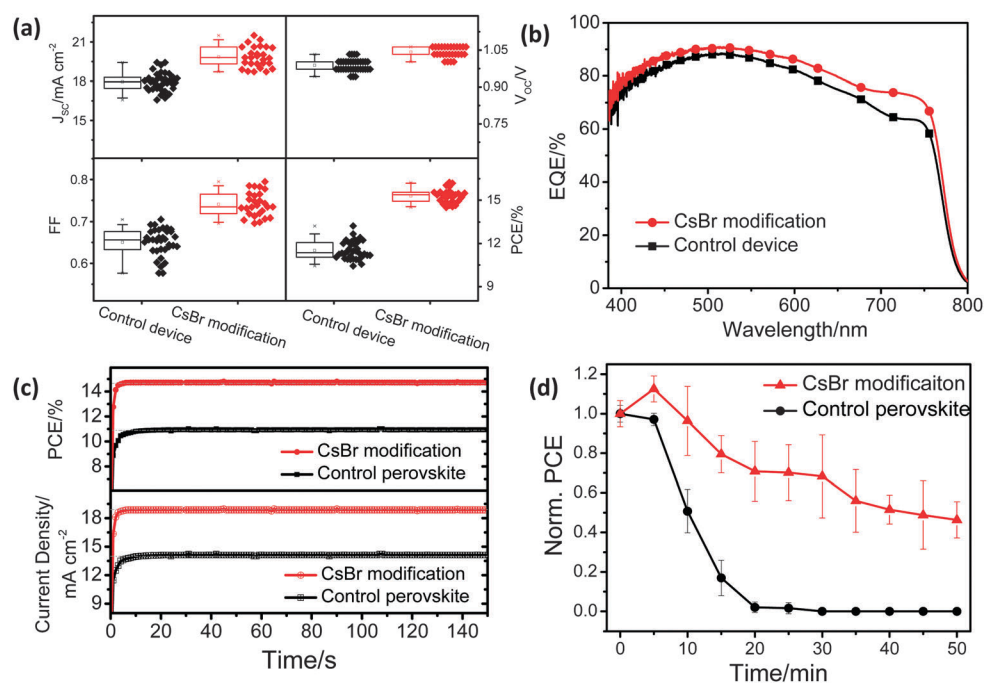

Fig. 5 (a) Device performance at optimised conditions with and without CsBr modification measured under simulated AM1.5 sunlight of 100 mW cm^{-2} irradiance. The data are represented for 62 data points as a standard box plot where the box range is defined by the s.d. Ninety percent of all data points fall within the upper and lower whiskers. (b) The EQE result for the device with and without CsBr modification, (c) the stabilized power output of the cell. (d) The normalized PCE decay of devices upon UV irradiation.

This journal is © The Royal Society of Chemistry 2016

Energy Environ. Sci., 2016, **9**, 490–498 | **495**

Table 1 Solar cell performance parameters

Samples		$J_{SC}{}^{a}$/mA cm^{-2}	$V_{OC}{}^{b}$/V	FF^{c}	PCE^{d}/%	SPO^{e}/%
CsBr average		19.8 ± 0.7	1.04 ± 0.02	0.74 ± 0.03	15.3 ± 0.5	14.7
CsBr champion	Forward	20.7	1.06	0.75	16.3	
	Reverse	20.6	0.90	0.63	11.5	
Control average		17.9 ± 0.7	0.98 ± 0.02	0.65 ± 0.03	11.5 ± 0.6	10.9
Control champion	Forward	18.7	0.99	0.69	13.1	
	Reverse	18.5	0.88	0.60	9.66	

^{a} J_{SC}, short-circuit current density. ^{b} V_{OC}, open circuit voltage. ^{c} FF, fill factor. ^{d} PCE, power conversion efficiency. ^{e} SPO, stabilized power output.

In Fig. 5b we presents the external quantum efficiency (EQE) spectra of devices without (control) and with CsBr modification. Compared with the control devices, CsBr modified devices exhibit a higher photo-response over the entire spectral region, but specifically enhanced near the band edge. Since the optical density at higher energies than the band edge is already greater than 1 for the control film, this panchromatic enhancement of EQE is most likely resulting from an electronic improvement of the solar cell, rather than improved light harvesting. As we presented in Fig. 3a, we have observed enhanced quenching of the PL for perovskite films processed on the CsBr modified c-TiO$_2$, and in addition enhanced lifetime of the perovskite films processed on glass. This is consistent with the CsBr modification reducing the density of non-radiative defect sites at the buried interface, whilst at the same time enhancing the rate of electron transfer across this interface. Accordingly charge extraction to the external circuit competes much more favourably with recombination losses in the CsBr modified devices *versus* the unmodified devices.

Finally, we investigated the stability of the perovskite films and complete solar cells under UV irradiation without encapsulation. This is a rather brutal test where we expect to observe degradation; however it helps to quickly identify if a fundamental enhancement in stability has been achieved. We exposed the cells to 365 nm 523 mW cm^{-2} UV illumination (equivalent to 113 suns equivalent of UV light below 400 nm in wavelength), and removed the cells at certain time intervals to measure the current voltage curves under simulated AM1.5 100 mW cm^{-2} irradiance. In Fig. 5d we observe that the devices with CsBr modification exhibit significantly improved stability. The normalized PCE remains more than 70% of its initial value even after 20 min UV irradiation in air. By contrast, the control device shows nearly zero PCE under the same exposure and testing conditions. Based on our UV-Vis and XRD results presented in Fig. 4, the perovskite is decomposed into PbI$_2$, with the degradation being driven by the interface between c-TiO$_2$ and perovskite. It may be the case that electron transfer is blocked if a thick layer of PbI$_2$ exists at the TiO$_2$ perovskite interface. A mechanism such as this could explain why the PCE for the control devices decreases rapidly even without any visible yellowing within the first 20 min. It may also be that along with the generation of PbI$_2$ there are a lot of other defects generated within the perovskite and specifically at the perovskite/c-TiO$_2$ interface. If these defects are electronic traps, then a drop off in performance could occur far earlier than the onset of degradation visible to the naked eye.

In addition to CsBr, we screened other candidates as interface modifiers, including MABr, CsCl and CsI, and we summarise the JV parameters with optimised concentration for each treatment in Fig. S9a (ESI†). Based on the optimised efficiency, we then tested the device stability under UV light exposure and show the result in Fig. S9b (ESI†). These results confirm that both CsBr and CsCl could enhance the device stability. However, we found that the initial device PCE is higher when employing CsBr rather than CsCl as the interface modifier. Therefore, the CsBr is a better choice than CsCl in terms of device PCE and stability. We note that from all the Cs halide and MA halide salts we tested, CsBr is the least soluble in DMF.

In Fig. 6a–d we further illustrate the degradation process of the devices without and with CsBr modification. During the UV light irradiation, the perovskite degrades, turning yellow with the conversion to PbI$_2$ (Fig. 6a and b). Our results are consistent with this degradation being induced by TiO$_2$ being in direct contact with the perovskite. We illustrate the CsBr modification at the interface of perovskite and the c-TiO$_2$ layer by the grey regions in Fig. 6c. After the UV irradiation, the CsBr layer protects the perovskite against UV-light induced photocatalytic decomposition from the c-TiO$_2$, without any obvious colour changes as we illustrate in Fig. 6d. We note that the primary function of the CsBr appears to be the inhibition of the photocatalytic activity of the TiO$_2$, but since the CsBr appears to form clusters as opposed to a continuous film, it is unlikely that CsBr acts as a buffer layer in the traditional sense, inhibiting contact between the TiO$_2$ and perovskite. Rather, it is likely that the Cs ions inhibit the photocatalytically active sites on the TiO$_2$,
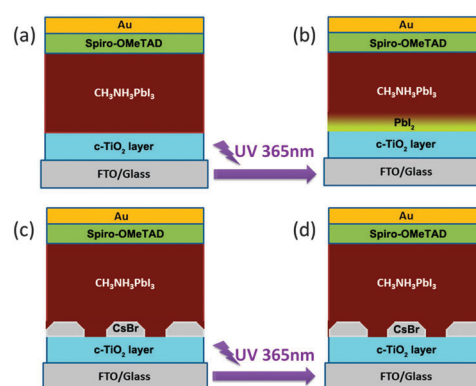

Fig. 6 Schematic illustration of the control perovskite solar cell (a) before and (b) after UV irradiation, and perovskite solar cell with CsBr interface modification (c) before and (d) after UV irradiation.

496 | *Energy Environ. Sci.*, 2016, **9**, 490–498

This journal is © The Royal Society of Chemistry 2016

and assist in the formation of less defective perovskite at this interface, as revealed by the reduced photocatalytic properties of TiO_2 after CsBr modification and the TAS measurements. The work we have presented here is related to short term degradation processes in the presence of UV light and air. In further work we will look into the impact of the CsBr interface modification upon the long term stability of solar cells encapsulated in inert environments.

Conclusions

In summary, we have demonstrated that CsBr can be effectively employed as an interface modifier between the c-TiO_2 and perovskite films in planar heterojunction solar cells. The CsBr modification not only improves the stabilized power conversion efficiency, but it also has a strongly positive impact upon the resilience of the perovskite solar cell to high levels of UV light exposure. Our results demonstrate that CsBr interfacial modification could be a key requirement in order to achieve long term stability of perovskite solar cells incorporating n-type TiO_2 or other metal oxides. We expect that future work focused towards understanding the short and long term performance enhancing mechanisms of this and other interface modifications will help to optimise the n-type collection layer/perovskite interface. Similar studies may also reveal benefits at the p-type collection layer/perovskite interface, especially in the "inverted perovskite" cells where the perovskite layer is crystallised directly on the p-type charge collection material.

Acknowledgements

Notes and references

1 P. B. Weisz, *Phys. Today*, 2004, **57**, 47–52.

2 M. S. Dresselhaus, G. W. Crabtree and M. V. Buchanan, *MRS Bull.*, 2005, **30**, 518–524.

3 L. Etgar, P. Gao, Z. Xue, Q. Peng, A. K. Chandiran, B. Liu, M. K. Nazeeruddin and M. Grätzel, *J. Am. Chem. Soc.*, 2012, **134**, 17396–17399.

4 M. M. Lee, J. Teuscher, T. Miyasaka, T. N. Murakami and H. J. Snaith, *Science*, 2012, **338**, 643–647.

5 G. Xing, N. Mathews, S. Sun, S. S. Lim, Y. M. Lam, M. Grätzel, S. Mhaisalkar and T. C. Sum, *Science*, 2013, **342**, 344–347.

6 M. Liu, M. B. Johnston and H. J. Snaith, *Nature*, 2013, **501**, 395–398.

7 J. H. Heo, S. H. Im, J. H. Noh, T. N. Mandal, C.-S. Lim, J. A. Chang, Y. H. Lee, H.-J. Kim, A. Sarkar, K. NazeeruddinMd, M. Gratzel and S. I. Seok, *Nat. Photonics*, 2013, **7**, 486–491.

8 J. Burschka, N. Pellet, S.-J. Moon, R. Humphry-Baker, P. Gao, M. K. Nazeeruddin and M. Gratzel, *Nature*, 2013, **499**, 316–319.

9 H. Zhou, Q. Chen, G. Li, S. Luo, T.-B. Song, H.-S. Duan, Z. Hong, J. You, Y. Liu and Y. Yang, *Science*, 2014, **345**, 542–546.

10 A. Kojima, K. Teshima, Y. Shirai and T. Miyasaka, *J. Am. Chem. Soc.*, 2009, **131**, 6050–6051.

11 H.-S. Kim, C.-R. Lee, J.-H. Im, K.-B. Lee, T. Moehl, A. Marchioro, S.-J. Moon, R. Humphry-Baker, J.-H. Yum, J. E. Moser, M. Gratzel and N.-G. Park, *Sci. Rep.*, 2012, **2**, 591.

12 W. Nie, H. Tsai, R. Asadpour, J.-C. Blancon, A. J. Neukirch, G. Gupta, J. J. Crochet, M. Chhowalla, S. Tretiak, M. A. Alam, H.-L. Wang and A. D. Mohite, *Science*, 2015, **347**, 522–525.

13 W. Zhang, M. Saliba, D. T. Moore, S. K. Pathak, M. T. Hörantner, T. Stergiopoulos, S. D. Stranks, G. E. Eperon, J. A. Alexander-Webber, A. Abate, A. Sadhanala, S. Yao, Y. Chen, R. H. Friend, L. A. Estroff, U. Wiesner and H. J. Snaith, *Nat. Commun.*, 2015, **6**, 6142.

14 D. Shi, V. Adinolfi, R. Comin, M. Yuan, E. Alarousu, A. Buin, Y. Chen, S. Hoogland, A. Rothenberger, K. Katsiev, Y. Losovyj, X. Zhang, P. A. Dowben, O. F. Mohammed, E. H. Sargent and O. M. Bakr, *Science*, 2015, **347**, 519–522.

15 Q. Dong, Y. Fang, Y. Shao, P. Mulligan, J. Qiu, L. Cao and J. Huang, *Science*, 2015, **347**, 967–970.

16 W. S. Yang, *et al.*, *Science*, 2015, **348**, 1234–1237.

17 J. Jean, P. R. Brown, R. L. Jaffe, T. Buonassisi and V. Bulovic, *Energy Environ. Sci.*, 2015, **8**, 1200–1219.

18 M. A. Green, K. Emery, Y. Hishikawa, W. Warta and E. D. Dunlop, *Progress in Photovoltaics: Research and Applications*, 2015, **23**, 1–9.

19 S. Shi, Y. Li, X. Li and H. Wang, *Mater. Horiz.*, 2015, **2**, 378–405.

20 M. A. Green, A. Ho-Baillie and H. J. Snaith, *Nat. Photonics*, 2014, **8**, 506–514.

21 C.-C. Chueh, C.-Z. Li and A. K. Y. Jen, *Energy Environ. Sci.*, 2015, **8**, 1160–1189.

22 G. Niu, X. Guo and L. Wang, *J. Mater. Chem. A*, 2015, **3**, 8970–8980.

23 A. M. Leguy, Y. Hu, M. Campoy-Quiles, M. I. Alonso, O. J. Weber, P. Azarhoosh, M. van Schilfgaarde, M. T. Weller, T. Bein, J. Nelson, P. Docampo and P. R. Barnes, *Chem. Mater.*, 2015, **27**, 3397–3407.

24 G. Niu, W. Li, F. Meng, L. Wang, H. Dong and Y. Qiu, *J. Mater. Chem. A*, 2014, **2**, 705–710.

25 W. Li, J. Li, L. Wang, G. Niu, R. Gao and Y. Qiu, *J. Mater. Chem. A*, 2013, **1**, 11735–11740.

26 J. H. Noh, S. H. Im, J. H. Heo, T. N. Mandal and S. I. Seok, *Nano Lett.*, 2013, **13**, 1764–1769.

27 I. C. Smith, E. T. Hoke, D. Solis-Ibarra, M. D. McGehee and H. I. Karunadasa, *Angew. Chem.*, 2014, **126**, 11414–11417.

28 S. N. Habisreutinger, T. Leijtens, G. E. Eperon, S. D. Stranks, R. J. Nicholas and H. J. Snaith, *Nano Lett.*, 2014, **14**, 5561–5568.

29 A. Mei, X. Li, L. Liu, Z. Ku, T. Liu, Y. Rong, M. Xu, M. Hu, J. Chen, Y. Yang, M. Grätzel and H. Han, *Science*, 2014, **345**, 295–298.

30 S. Ito, S. Tanaka, K. Manabe and H. Nishino, *J. Phys. Chem. C*, 2014, **118**, 16995–17000.

31 T. Leijtens, G. E. Eperon, S. Pathak, A. Abate, M. M. Lee and H. J. Snaith, *Nat. Commun.*, 2013, **4**, 2885.

32 K. Wojciechowski, S. D. Stranks, A. Abate, G. Sadoughi, A. Sadhanala, N. Kopidakis, G. Rumbles, C.-Z. Li, R. H. Friend, A. K. Y. Jen and H. J. Snaith, *ACS Nano*, 2014, **8**, 12701–12709.

33 K. Wojciechowski, T. Leijtens, S. Siprova, C. Schlueter, M. T. Hörantner, J. T.-W. Wang, C.-Z. Li, A. K. Y. Jen, T.-L. Lee and H. J. Snaith, *J. Phys. Chem. Lett.*, 2015, **6**, 2399–2405.

34 Q. Hu, J. Wu, C. Jiang, T. Liu, X. Que, R. Zhu and Q. Gong, *ACS Nano*, 2014, **8**, 10161–10167.

35 W. Zhang, M. Anaya, G. Lozano, M. E. Calvo, M. B. Johnston, H. Míguez and H. J. Snaith, *Nano Lett.*, 2015, **15**, 1698–1702.

36 J. Manassen, D. Cahen, G. Hodes and A. Sofer, *Nature*, 1976, **263**, 97–100.

37 D. Cahen and A. Kahn, *Adv. Mater.*, 2003, **15**, 271–277.

38 H. P. Dong, Y. Li, S. F. Wang, W. Z. Li, N. Li, X. D. Guo and L. D. Wang, *J. Mater. Chem. A*, 2015, **3**, 9999–10004.

39 H. Choi, J. Jeong, H.-B. Kim, S. Kim, B. Walker, G.-H. Kim and J. Y. Kim, *Nano Energy*, 2014, **7**, 80–85.

40 G. E. Eperon, V. M. Burlakov, A. Goriely and H. J. Snaith, *ACS Nano*, 2014, **8**, 591–598.

41 V. D'Innocenzo, A. R. Srimath Kandada, M. De Bastiani, M. Gandini and A. Petrozza, *J. Am. Chem. Soc.*, 2014, **136**, 17730–17733.

42 T. Sakuma, M. Mutou, K. Ohki, M. Arai, H. Takahashi and Y. Ishii, *Solid State Ionics*, 2002, **154–155**, 237–242.

43 C. C. Stoumpos, C. D. Malliakas and M. G. Kanatzidis, *Inorg. Chem.*, 2013, **52**, 9019–9038.

44 G. E. Eperon, S. D. Stranks, C. Menelaou, M. B. Johnston, L. M. Herz and H. J. Snaith, *Energy Environ. Sci.*, 2014, **7**, 982–988.

45 S. D. Stranks, G. E. Eperon, G. Grancini, C. Menelaou, M. J. P. Alcocer, T. Leijtens, L. M. Herz, A. Petrozza and H. J. Snaith, *Science*, 2013, **342**, 341–344.

46 J. You, Z. Hong, Y. Yang, Q. Chen, M. Cai, T.-B. Song, C.-C. Chen, S. Lu, Y. Liu, H. Zhou and Y. Yang, *ACS Nano*, 2014, **8**, 1674–1680.

47 T. Yajima, M. Minohara, C. Bell, H. Kumigashira, M. Oshima, H. Y. Hwang and Y. Hikita, *Nano Lett.*, 2015, **15**, 1622–1626.

48 Y. Shao, Z. Xiao, C. Bi, Y. Yuan and J. Huang, *Nat. Commun.*, 2014, **5**, 5784.

49 H. Duan, H. Zhou, Q. Chen, P. Sun, S. Luo, T. Song, B. Bob and Y. Yang, *Phys. Chem. Chem. Phys.*, 2015, **17**, 112–116.

50 X. Dong, X. Fang, M. Lv, B. Lin, S. Zhang, J. Ding and N. Yuan, *J. Mater. Chem. A*, 2015, **3**, 5360–5367.

51 C. Burda, Y. Lou, X. Chen, A. C. Samia, J. Stout and J. L. Gole, *Nano Lett.*, 2003, **3**, 1049–1051.

52 S. Reenen, M. Kemerink and H. J. Snaith, *J. Phys. Chem. Lett.*, 2015, **6**, 3808–3814.

53 H. J. Snaith, A. Abate, J. M. Ball, G. E. Eperon, T. Leijtens, N. K. Noel, S. D. Stranks, J. T.-W. Wang, K. Wojciechowski and W. Zhang, *J. Phys. Chem. Lett.*, 2014, **5**, 1511–1515.

498 | *Energy Environ. Sci.*, 2016, **9**, 490–498

This journal is © The Royal Society of Chemistry 2016